

Atomic Models by Cryo-EM and Site-Directed Spin Labeling: Application to the N-Terminal Region of Hsp16.5

Hanane A. Koteiche,¹ Steve Chiu,²
Rebecca L. Majdich,¹ Phoebe L. Stewart,^{1,2,*}
and Hassane S. Mchaourab^{1,*}

¹Department of Molecular Physiology and Biophysics
Center for Structural Biology
Vanderbilt University Medical Center
Nashville, Tennessee 37232

²Department of Molecular and Medical Pharmacology
Crump Institute for Molecular Imaging
David Geffen School of Medicine
University of California, Los Angeles
Los Angeles, California 90095

Summary

We report an approach for determining the structure of macromolecular assemblies by the combined application of cryo-electron microscopy (cryo-EM) and site-directed spin labeling electron paramagnetic resonance spectroscopy (EPR). This approach is illustrated for Hsp16.5, a small heat shock protein that prevents the aggregation of nonnative proteins. The structure of Hsp16.5 has been previously studied by both cryo-EM and X-ray crystallography. The crystal structure revealed a roughly spherical protein shell with dodecameric symmetry; however, residues 1–32 were found to be disordered. The cryo-EM reconstruction at 13 Å resolution appeared similar to the crystal structure but with additional internal density corresponding to the N-terminal regions of the 24 subunits. In this study, a systematic application of site-directed spin labeling and EPR spectroscopy was carried out. By combining the EPR constraints from spin label accessibilities and proximities with the cryo-EM density, we obtained an atomic model for a portion of the Hsp16.5 N-terminal region in the context of the oligomeric complex.

Introduction

Principal cellular processes such as transcription, signal transduction, and protein folding are often mediated by macromolecular assemblies consisting of multiple proteins or oligomers. Structural insight into these subcellular molecular machines is challenging as they are not always amenable to crystallization and their large size precludes the use of nuclear magnetic resonance spectroscopy. Also, crystallography cannot always resolve flexible regions that may be important for biological activity.

Among the complexes involved in protein folding are multiple families of heat shock proteins or molecular chaperones (Parsell and Lindquist, 1993). Our laboratories are interested in determining the structures of the small heat shock proteins (sHSPs), a superfamily of

heat-induced proteins of 12–40 kDa subunit size (MacRae, 2000). These monomers assemble into oligomeric complexes ranging from 4 to 40 subunits with divergent symmetries and substantially different degrees of order. For example, recombinant human α B-crystallin has been shown by cryo-EM imaging to have a variable quaternary structure without symmetry (Haley et al., 1998), whereas Hsp16.5 from the hyperthermophile *Methanococcus jannaschii* has been crystallized and has octahedral symmetry (Kim et al., 1998). Insight into the structure of sHSPs is limited primarily by the intrinsic flexibility and polydispersity of their oligomers. Consequently, the structural basis of their function is poorly understood.

We describe an approach for building atomic models of macromolecular complexes that combines the global perspective provided by cryo-electron microscopy (cryo-EM; Frank, 2002) with site-specific information derived from site-directed spin labeling (SDSL) and electron paramagnetic resonance spectroscopy (EPR) (Hubbell et al., 2000). The method involves experimentally determining secondary structure, solvent accessibility, and side chain proximities and using this information to thread the amino acid sequence into a cryo-EM density map. We illustrate this approach with the flexible N-terminal region of Hsp16.5. The crystal structure of Hsp16.5 reveals a symmetrical complex of 24 subunits with a hollow interior and windows at the 3-fold symmetry axes (Kim et al., 1998). The N-terminal 32 residues are highly disordered and are unresolved in the crystal structure. The potential involvement of this region in substrate binding (van Montfort et al., 2001) makes its structure determination critical for a mechanistic understanding of Hsp16.5 chaperone activity.

Results and Discussion

EPR constraints were derived from analysis of 40 spin-labeled mutants introduced individually along the length of the Hsp16.5 N-terminal region. Overall, the EPR data reflect a sterically packed, solvent-inaccessible environment. We observed broadening of varying extents in the spectral EPR line shapes that arises from spin-spin interactions between nitroxides in close proximity (Figure 1A). Furthermore, the line shapes from spin-diluted oligomers, obtained by refolding the spin-labeled subunits in the presence of excess unlabeled wild-type, were uniformly indicative of nitroxides undergoing restricted motion similar to those in the hydrophobic cores of monomeric proteins. A cryo-EM reconstruction of Hsp16.5 reveals density in the interior of the complex with a volume appropriate for 24 copies of the N-terminal region (Haley et al., 2000). The EPR results support the assignment of this density to the N-terminal region.

To determine solvent accessibility and sequence-specific secondary structure, we measured the EPR accessibility parameter, Π , of the nitroxide side chains to the water-soluble paramagnetic reagents nickel (II)

*Correspondence: hassane.mchaourab@vanderbilt.edu (H.S.M.); phoebe.stewart@vanderbilt.edu (P.L.S.)

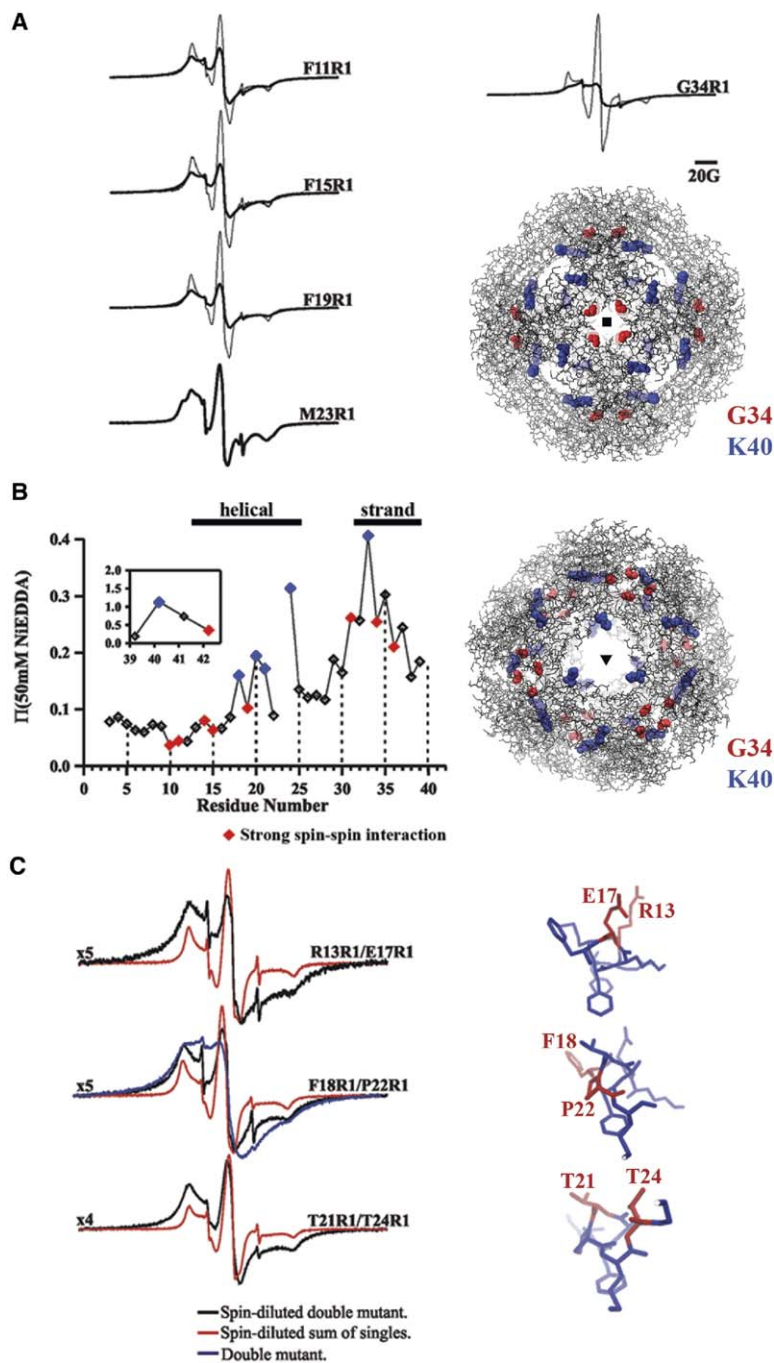


Figure 1. EPR Data for the N-Terminal Region of Hsp16.5

(A) Representative spectra showing broadening due to spin-spin interactions (dark trace) and restricted motion of the nitroxide side chain in the spin-diluted form (light trace). The spectra and location of G34 (red) in the crystal structure (Protein Data Bank code 1SHS, biological 24-fold assembly) are shown for reference.

(B) Accessibility profile to 50 mM NiEDDA, with blue symbols representing the residues at local accessibility maxima and red symbols indicating the residues with the strongest spin-spin interactions. The accessibility of residues 33–42 in the crystal structure and the position of K40 (blue) near a 3-fold window are shown for reference.

(C) EPR spectra of $i,i+3$ and $i,i+4$ residue pairs (left). The reduced signal amplitude of the spin-diluted double-mutant spectrum relative to the spin-diluted sum of single mutants is reflected by the scaling factor. For the 18/21 pair the undiluted spectrum is also shown (blue). The atomic model for residues 6–25 is viewed along the helical axis and with the corresponding residue pairs highlighted (right). Graphics representations were produced with Chimera (Pettersen et al., 2004) and DINO (<http://www.dino3d.org>).

ethylenediamine-diacetate (NiEDDA) and O_2 . In the presence of 20% O_2 or 3 mM NiEDDA, the absolute value of Π is small and the sequence-correlated contrast in many regions is within the experimental error, confirming that the entire region is in a buried, sterically restrictive environment (data not shown). Π (NiEDDA) at a concentration of 50 mM shows a gradient of increasing accessibility as the nitroxide is moved from the N terminus toward the α -crystallin domain (Figure 1B). Residue K40, which is solvent accessible at the 3-fold window in the crystal structure, has a NiEDDA accessi-

bility parameter, Π , more than ten times greater than the average of the first ten residues. Within the NiEDDA accessibility profile, two periodic patterns indicative of secondary structure are apparent. Between residues 32 and 39, Π oscillates with a periodicity of 2, consistent with the β strand observed in the crystal structure (residues 36–40). In the residue stretch 13–25, Π varies with a periodicity that approximates 3.6, suggesting a helical configuration. This is in agreement with the PSIPRED (McGuffin et al., 2000) prediction of an α helix for the overlapping residues (6–19). The helical and the β

strand regions are connected by a short stretch of residues where Π lacks a clear pattern, indicating either a loop or a segment of secondary structure that does not sample two distinct environments.

EPR constraints were also derived from spin label pairs introduced in the 13–24 segment in order to confirm a helical configuration for this region. The EPR spectra of pairs separated by one turn ($i,i+3$ and $i,i+4$) are extensively broadened in the spin-diluted form, indicating intrasubunit proximity (Figure 1C). In contrast, spin dilution eliminates the broadening in $i,i+2$ pairs such as 13/15 and 18/20, predicted to be on opposite sides of an α helix (data not shown). The spin label pair data support a helical configuration for residues 13–24. In constructing the model, we assumed that the proline at position 22 ends the α helix. However, the backbone conformation between residues 22 and 24 was constrained to be a turn, as the EPR spectrum of the 21/24 pair indicates close proximity between these residues.

Because the spectral broadening illustrated in Figure 1A may arise from the proximity of more than two spin labels, the extent of spin-spin interactions was ranked by the reduction in the intensity of the central line in the fully labeled oligomer relative to the spin-diluted one. For reference, Figure 1A also shows the spectrum of residue 34, which is visible in the crystal structure and located at the 4-fold symmetry axis. The side chains in the N-terminal region ranked to be closest to their symmetry-related sites are 10, 11, 14, 15, 19, 23, and 31. These proximities provide a set of spatial constraints that reflect the relative packing of the subunits.

We built an atomic model for residues 6–25 that fits within the cryo-EM density, agrees well with the EPR constraints, and has backbone torsion angles within favored Ramachandran regions. The cryo-EM reconstruction of Hsp16.5 displays 24 well-separated tubes of density that are suggestive of α helices and that are solvent accessible at the 3-fold symmetry axes (Haley et al., 2000). Cropping the cryo-EM density perpendicular to a 4-fold symmetry axis reveals eight density tubes all approximately in the same plane. The N-terminal model fits within one density tube (Figure 2A). Imposing octahedral symmetry on the model produces a pseudoatomic model for 24 symmetry-related copies of residues 6–25. When the crystal structure for the outer protein shell and the pseudoatomic model for the N-terminal region are both displayed as density maps filtered to 13 Å resolution, the two maps together provide a good approximation to the cryo-EM reconstruction of the oligomer (Figures 2A and 2B).

The quantitative docking tool CoLoRes in the Situs software package (Chacón and Wriggers, 2002) was used to calculate the correlation of the cryo-EM density map with the oligomeric form of the crystallographic and model coordinates. Inclusion of the N-terminal model leads to an increase of 20% in the correlation with the cryo-EM density, consistent with the increase of 17% in the number of residues. This result confirms our visual assessment that the model fits well within the cryo-EM density.

Polypeptide backbone $C\alpha$ trace representations of the crystal structure and the pseudoatomic model for the oligomer show that four N-terminal helices are in close proximity at the 4-fold symmetry axes (Figure 2C).

When the oligomer is viewed along a 3-fold symmetry axis, three helices are visible within the 3-fold opening of the outer protein shell. Residues 11, 15, 19, and 23 are positioned such that their side chains point toward the 4-fold symmetry axes (Figure 3A), in agreement with the EPR spin-spin interaction data. Two additional residues with strong spin-spin interactions, 10 and 14, are positioned such that their side chains are in close proximity where three helices meet at the 3-fold axis.

To assess the fit between the EPR distance constraints and the model, coordinates were generated to approximate the distal end of a spin label attached to each residue. For this computation, the spin label was assumed to extend 7 Å from the $C\alpha$ atom along the $C\alpha$ - $C\beta$ bond vector (Rabenstein and Shin, 1995). Twenty-three pairwise distances were calculated for each site and the distance of closest approach is plotted in Figure 3B as a function of residue number. Minima are observed at residues 10, 15, 19, and 23, which are observed by EPR to have strong spin-spin interactions. In addition, the closest approach distances calculated for residues 11 and 14, while not minima, are less than 10 Å, in accord with the observed strong spin-spin interactions for these sites. Thus, the calculated distances from the N-terminal pseudoatomic model are in good agreement with pattern of experimental intermonomer spin-spin interactions.

Similar calculations were carried out for the intramonomer nitroxide pairs (Figure 1C). A distance of 8 Å was found for the 13/17 pair, 10 Å for the 18/22 pair, and 14 Å for the 21/24 pair. These distances are consistent with the observed strong spin-spin interactions at these pairs. The model yields distances of 16 Å for both of the pairs (13/15 and 18/20) characterized by weak spin-spin interactions.

To validate some of the assumptions built into our approximation of the spin label positions, we applied the same calculation to three residues in the crystal structure that are also observed to have strong spin-spin interactions (residues 34, 36, and 42) (Koteiche and Mchaourab, 2002). Of these three residues, G34 has the strongest interaction. The distance calculation yielded 3, 9, and 10 Å, respectively, for the closest approach distance for spin labels on these residues. Therefore, we conclude that the approximations used in calculating the spin label positions are reasonable.

The residues within the N-terminal region with the highest accessibilities to NiEDDA (residues 18, 20, 21, and 24) are positioned such that their side chains form a ridge along the surface of the helix that is exposed in the 3-fold openings of the protein shell (Figure 3C). Mapping the Π (NiEDDA) values on the surface of the model reveals the qualitative agreement between the model and the experimental solvent accessibility data. The agreement was confirmed by calculation of the fractional solvent accessibility (f_{SA}) for the native side chains of the pseudoatomic model within the context of the oligomeric crystal structure. For the most part, the calculated local maxima corresponded with the experimental maxima; however, the calculation did not reproduce the amplitude gradient observed in Figure 1B. For instance, the f_{SA} of residue 18 is ~3-fold larger than that of residue 40, which clearly disagrees with the experimental data. In addition, the native side chain of

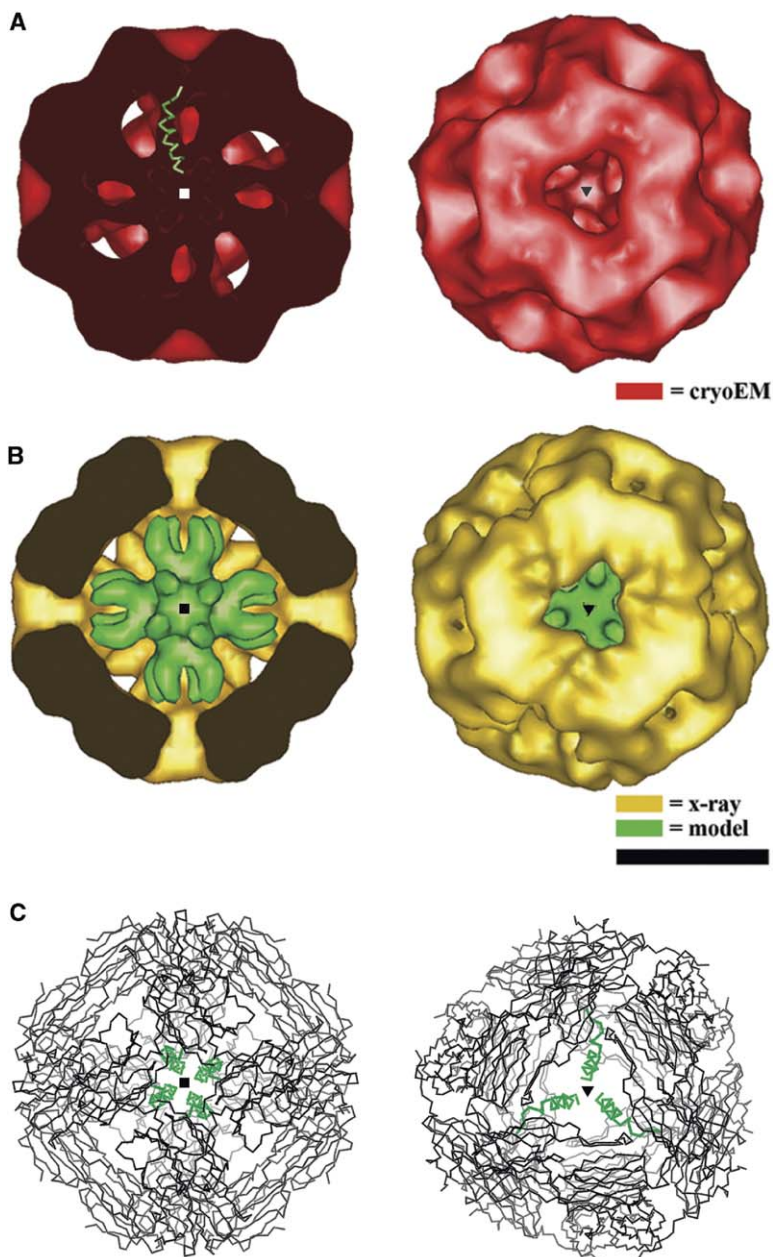


Figure 2. Agreement between the Cryo-EM Density and the Combined Crystallographic and Pseudoatomic Model Coordinates

(A) Cryo-EM reconstruction of Hsp16.5 at 13 Å resolution cropped (left) and in full (right). The model for residues 6–25 (green) is positioned within one tube of density.

(B) The crystal structure (yellow) together with the pseudoatomic model for the N-terminal region (green) both filtered to 13 Å. The scale bar (black) represents 50 Å.

(C) Backbone C α trace representations of the crystal structure (amino acids 33–147, black) together with selected copies of the N-terminal model (amino acids 6–25, green) clustered at either a 4-fold (left) or a 3-fold symmetry axis (right). The 3-fold and 4-fold symmetry axes are represented by white or black triangles and squares, respectively. Graphics representations were produced with AVS5 and Chimera.

T24 is too short to reach into the 3-fold opening and therefore the calculated f_{SA} is not as high as would be expected for a longer spin label side chain. Previous studies of monomeric proteins with known crystal structures revealed a poor quantitative correlation between Π and f_{SA} that was attributed primarily to the difference in molar size between the native and spin label side chains (Isas et al., 2002). For an oligomeric protein, an added confounding factor is the dependence of the EPR accessibility parameter on the reagent concentration and its diffusion coefficient. In the case of Hsp16.5, the increase in steric restriction toward the center of the particle presumably reduces the concentration/diffusion product of NiEDDA, thus leading to the observed gradient in accessibility. Gradients

of oxygen accessibility are routinely observed in SDSL of transmembrane helices as the concentration/diffusion product of oxygen progressively increases toward the middle of the bilayer (Hubbell et al., 2000).

In generating the N-terminal model, a canonical α helix was used as the starting model for residues 6–22. The model was positioned manually within the cryo-EM density for the best subjective agreement with the EPR data. Next, the backbone torsion angles of the model were adjusted for improved visual agreement with the EPR constraints and the cryo-EM density. Throughout this process, the backbone torsion angles for residues 6–19 were kept within $\pm 20^\circ$ of the canonical α -helical values, because both the EPR data and secondary structure predictions are consistent with an α helix in

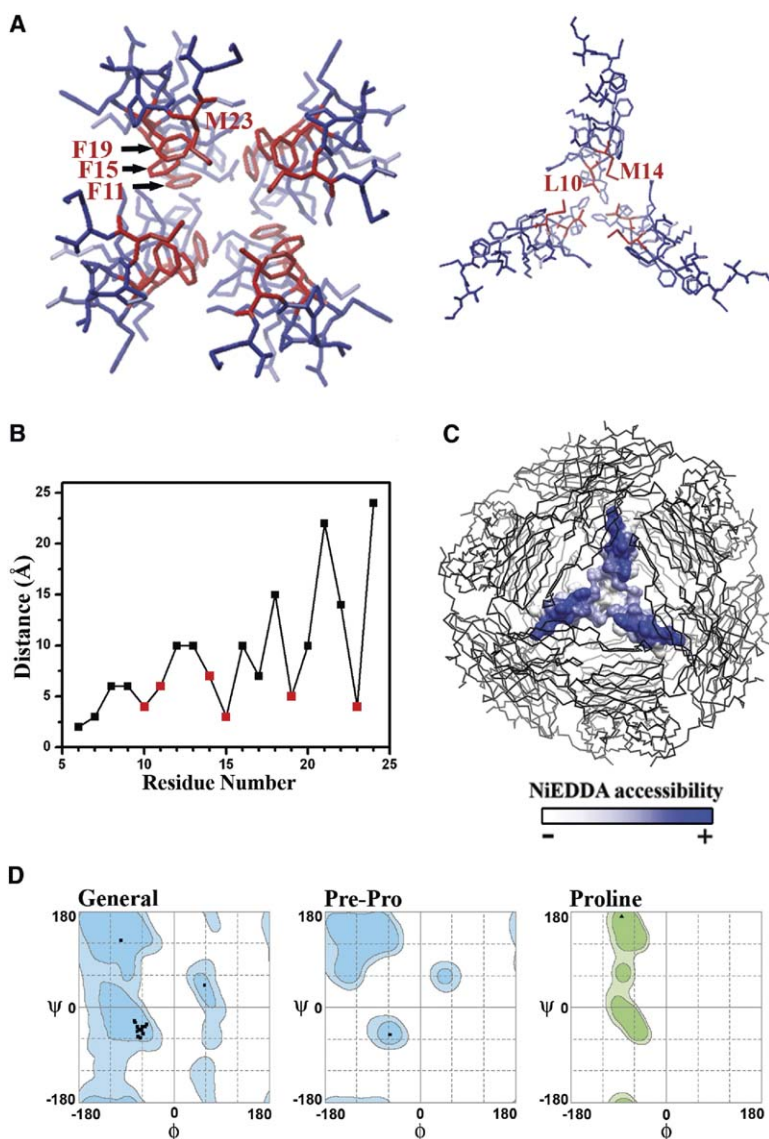


Figure 3. Assessment of the Model

(A) The side chains clustered near a 4-fold axis (left) or a 3-fold axis (right) are indicated in red.

(B) Distance of closest approach between symmetry-related copies of each residue in the N-terminal pseudoatomic model. The positions observed by EPR to have the strongest spin-spin interactions are indicated by red symbols.

(C) Π (NiEDDA) mapped onto a molecular surface of three selected copies of the N-terminal model and shown together with a backbone $C\alpha$ trace representation of the crystal structure (black).

(D) Ramachandran plots of the backbone torsion angles in the N-terminal model shown in three panels for general residues (left); the preproline residue T21 (middle); and the proline residue P22 (right). Note that only residues P22, M23, and T24 have backbone torsion angles outside of the α -helical region. The color-saturated regions represent the favored regions for each residue type. The plots were created by the RAMPAGE Ramachandran Plot Assessment server (<http://raven.bioc.cam.ac.uk/rampage>; Lovell et al., 2003).

this region. For residues 20–24, all combinations of favored Ramachandran regions were evaluated. A coarse sampling was performed by moving the backbone torsion angles for each residue to the center of each allowed region within the Ramachandran plots for general, pre-Pro, and Pro residues, as appropriate for that particular residue. All but one of the possible structures could be ruled out by a visual qualitative assessment of the agreement with the experimental cryo-EM and EPR data. Finally, the backbone torsion angles of the selected structure were adjusted for optimal qualitative agreement with the data while keeping the angles within the chosen favorable Ramachandran regions (Figure 3D).

For a segment of secondary structure, such as an α helix, the overall positioning of the model, adjustment of backbone torsion angles, and comparison with EPR constraints can be performed manually as we have demonstrated. However, for more complex structures, which we expect to be the primary targets for this ap-

proach, this task quickly becomes daunting because of the large number of possible backbone structures. Therefore, we envision the development of a computational approach that would generate models for a given polypeptide region and apply a penalty function to evaluate agreement with the cryo-EM density and the EPR constraints. Clearly, the computational approach should include calculation of the f_{SA} of nitroxide side chains, rather than native side chains. With an automated strategy, it would be possible to generate families of structures and then carry out an iterative process of experimental validation where constraints are obtained to distinguish between various models. Such a computational approach would also provide a statistical assessment of the fit to the experimental constraints and would reveal where any uncertainties lie in the final model.

This report demonstrates a novel approach for determining the structure of macromolecular assemblies. While it is feasible to build atomic models from EPR

(Koteiche and Mchaourab, 1999; Perozo et al., 1998; Poirier et al., 1998) or cryo-EM (Miyazawa et al., 2003; Yonekura et al., 2003) data alone, the synergistic application of both methods reduces the number of EPR constraints that are needed and extends the resolution range for which cryo-EM density may be interpreted at the level of amino acid position. In addition to a cryo-EM single-particle reconstruction, this approach requires the systematic introduction of nitroxide side chains and EPR analysis in the region of interest. A moderate-resolution cryo-EM structure provides the global perspective that defines the organization of a complex or oligomer, while the site-specific information obtained from EPR analysis tends to be primarily local and results in defining the sequence-specific secondary structure, but not necessarily the relative packing of these elements. By combining the two techniques, the local EPR constraints provide the information necessary to thread the amino acid sequence within a moderate-resolution cryo-EM density map and to build an atomic model.

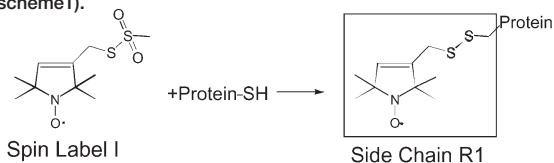
Experimental Procedures

Site-Directed Mutagenesis

Site-directed mutagenesis was performed using PCR methods including overlap extension and the megaprimer method (Koteiche and Mchaourab, 2002). The mutant plasmids were sequenced to confirm the substitution and the absence of unwanted changes.

Expression, Purification, and Spin Labeling of the Mutants

Hsp16.5 wild-type and mutants were expressed and purified as described previously (Koteiche and Mchaourab, 2002). Briefly, Hsp16.5 mutant plasmids were transformed into competent *Escherichia coli* BL21 (DE3). Cultures inoculated from overnight seeds were grown at 37°C until OD600 = 0.7–0.9 and induced by the addition of 0.4 mM isopropyl- β -D-thiogalactopyranoside (IPTG). After 3 hr induction at 37°C, the cells were harvested by centrifugation, resuspended into the lysis buffer, disrupted by sonication, and the DNA precipitated by the addition of 0.06% polyethyleneimine. Hsp16.5 variants were purified by anion exchange on a source Q column. Ammonium sulfate was added to the eluted anion exchange peak to a final concentration of 1 M, and the sample was then loaded on a phenyl sepharose column and eluted with a gradient of 1 M–0 M ammonium sulfate. The purified sample was loaded on a Superose 6 column followed by reaction with a 10-fold excess of the methanethiosulfonate spin label (MTSSL) for 2 hr at room temperature (Berliner et al., 1982). The reaction was allowed to proceed to completion overnight at 4°C to yield the side chain R1 (scheme1).



Single-site mutants are named by specifying the original residue, the number of the residue followed by R1.

Spin Dilution by Reconstitution of Mixed Hsp16.5 Oligomers

To measure the EPR accessibility parameter Π , Hsp16.5 mutant proteins were mixed at a ratio of 1 to 3 with wild-type Hsp16.5 in a buffer containing guanidine HCl at a concentration >5.5 M. After incubation for 20 min at room temperature, the samples were desalted into a buffer containing 20 mM MOPS, 50 mM NaCl (pH 7.2), and concentrated. This protocol eliminated the spectral feature arising from spin-spin interactions except for M23, where the spin-labeled subunits preferentially self-associate regardless of the molar excess of wild-type subunit.

Electron Paramagnetic Resonance Measurements

The samples for EPR spectroscopy were prepared in 20 mM MOPS, 50 mM NaCl, 0.1 mM EDTA (pH 7.2). EPR spectra were collected on a Bruker E500 spectrometer equipped with a super High Q cavity (Bruker Biospin, Billerica, MA). The microwave power was 5 mW; modulation amplitude was 1.6 G.

Power saturation measurements were carried out on a Varian E102 spectrometer (Varian, Palo Alto, CA) equipped with a two-loop one-gap resonator. The experiments were done under nitrogen, in the presence of 20% molecular oxygen or 3 mM or 50 mM NIEDDA. The data were then fitted to obtain the parameter $P_{1/2}$. The EPR accessibility parameter Π was calculated as previously described (Hubbell et al., 2000).

Size Exclusion Chromatography

The average molecular mass for all mutants was determined using size exclusion chromatography (SEC) on a Superose 6 column calibrated with a set of proteins of known molecular weights. All samples were injected from a 100 μ l sample volume at a flow rate of 0.5 ml/min. Both fully labeled and spin-diluted oligomers have retention times similar to that of the wild-type, indicating little if any perturbation by the cysteine substitution and subsequent labeling.

Atomic Model Building

The initial model was positioned within the cryo-EM reconstruction of Hsp16.5 (Haley et al., 2000) using the AVS5 visualization software package (Advanced Visual Systems, Waltham, MA). The backbone torsion angles were adjusted with Swiss-PdbViewer (<http://www.expasy.org/spdbv/>; Guex and Peitsch, 1997). A Fortran program (pdb2p) was used to convert atomic coordinates into a $C\alpha$ backbone representation that could be displayed along with the cryo-EM density in AVS5. Octahedral symmetry was applied to the model coordinates with a Fortran program (octrot). Microsoft Excel was used to calculate approximate coordinates for the distal end of the spin-labeled side chain R1 at each residue within the N-terminal model, assuming that the side chain R1 extends 7 Å from the $C\alpha$ atom along the $C\alpha$ -C β bond vector. Excel was used to calculate the closest approach distances for each site in the oligomeric pseudoatomic model and between intramonomer nitroxide pairs. The pseudoatomic model and crystallographic coordinates were converted to density maps and filtered to the same resolution as the cryo-EM reconstruction (13 Å) using Fortran programs (coord-60 and fermi-128). Energy minimization was performed with Swiss-PdbViewer. The model and crystal structure (Kim et al., 1998) were evaluated together with InsightII (Accelrys, San Diego, CA) and Chimera (Pettersen et al., 2004). The fractional solvent accessibility (f_{SA}) was calculated with the Homology module of the InsightII suite using the method of Lee and Richards (1971). The backbone torsion angles of the final model were evaluated by the RAMPAGE Ramachandran Plot Assessment server (<http://raven.bioc.cam.ac.uk/rampage/>; Lovell et al., 2003). The graphics figures were prepared with Chimera (Pettersen et al., 2004), DINO (<http://www.dino3d.org>), and AVS5.

Model Assessment

The limitations in the positioning of the helix within the cryo-EM density were assessed by generating translated and rotated versions of the model. Shifting the model by ± 5 Å along the helical axis resulted in either severe nonbonded clashes between model subunits after imposing octahedral symmetry or in clashes of the model with the outer protein shell of the crystal structure. Shifting the model by ± 5 Å perpendicular to the helical axis resulted in model density that was significantly offset from the density tubes in the cryo-EM reconstruction. Rotating the model by $\pm 30^\circ$ around the helical axis resulted in side chain positions that were less compatible with the EPR constraints. This is reasonable, as a rotation of 100° , together with an axial translation of ~ 1.5 Å, would result in shifting one side chain to the position of the next side chain in a canonical α helix.

Acknowledgments

This work was supported by grants from the National Institutes of Health (R01-EY12683 to H.S.M.; T32-GM008652 to S.C.) and from the National Science Foundation (MCB-9722353 to P.L.S.). The au-

thors thank Professor Joseph Horwitz for stimulating discussions and Professors Al Beth and Dave Piston for critical reading of the manuscript.

Received: February 11, 2005

Revised: April 18, 2005

Accepted: May 6, 2005

Published: August 9, 2005

References

- Berliner, L.J., Grunwald, J., Hankovszky, H.O., and Hideg, K. (1982). A novel reversible thiol-specific spin label: papain active site labeling and inhibition. *Anal. Biochem.* *119*, 450–455.
- Chacón, P., and Wriggers, W. (2002). Multi-resolution contour-based fitting of macromolecular structures. *J. Mol. Biol.* *317*, 375–384.
- Frank, J. (2002). Single-particle imaging of macromolecules by cryo-electron microscopy. *Annu. Rev. Biophys. Biomol. Struct.* *31*, 303–319.
- Guex, N., and Peitsch, M.C. (1997). SWISS-MODEL and the Swiss-PdbViewer: an environment for comparative protein modeling. *Electrophoresis* *18*, 2714–2723.
- Haley, D.A., Horwitz, J., and Stewart, P.L. (1998). The small heat-shock protein, α B-crystallin, has a variable quaternary structure. *J. Mol. Biol.* *277*, 27–35.
- Haley, D.A., Bova, M.P., Huang, Q.L., Mchaourab, H.S., and Stewart, P.L. (2000). Small heat-shock protein structures reveal a continuum from symmetric to variable assemblies. *J. Mol. Biol.* *298*, 261–272.
- Hubbell, W.L., Cafiso, D.S., and Altenbach, C. (2000). Identifying conformational changes with site-directed spin labeling. *Nat. Struct. Biol.* *7*, 735–739.
- Isas, J.M., Langen, R., Haigler, H.T., and Hubbell, W.L. (2002). Structure and dynamics of a helical hairpin and loop region in annexin 12: a site-directed spin labeling study. *Biochemistry* *41*, 1464–1473.
- Kim, K.K., Kim, R., and Kim, S.H. (1998). Crystal structure of a small heat-shock protein. *Nature* *394*, 595–599.
- Koteiche, H.A., and Mchaourab, H.S. (1999). Folding pattern of the α -crystallin domain in α A-crystallin determined by site-directed spin labeling. *J. Mol. Biol.* *294*, 561–577.
- Koteiche, H.A., and Mchaourab, H.S. (2002). The determinants of the oligomeric structure in Hsp16.5 are encoded in the α -crystallin domain. *FEBS Lett.* *519*, 16–22.
- Lee, B., and Richards, F.M. (1971). The interpretation of protein structures: estimation of static accessibility. *J. Mol. Biol.* *55*, 379–400.
- Lovell, S.C., Davis, I.W., Arendall, W.B. III, de Bakker, P.I., Word, J.M., Prisant, M.G., Richardson, J.S., and Richardson, D.C. (2003). Structure validation by $C\alpha$ geometry: Φ, Ψ and $C\beta$ deviation. *Proteins* *50*, 437–450.
- MacRae, T.H. (2000). Structure and function of small heat shock/ α -crystallin proteins: established concepts and emerging ideas. *Cell. Mol. Life Sci.* *57*, 899–913.
- McGuffin, L.J., Bryson, K., and Jones, D.T. (2000). The PSIPRED protein structure prediction server. *Bioinformatics* *16*, 404–405.
- Miyazawa, A., Fujiyoshi, Y., and Unwin, N. (2003). Structure and gating mechanism of the acetylcholine receptor pore. *Nature* *423*, 949–955.
- Parsell, D.A., and Lindquist, S. (1993). The function of heat-shock proteins in stress tolerance: degradation and reactivation of damaged proteins. *Annu. Rev. Genet.* *27*, 437–496.
- Perozo, E., Cortes, D.M., and Cuello, L.G. (1998). Three-dimensional architecture and gating mechanism of a K^+ channel studied by EPR spectroscopy. *Nat. Struct. Biol.* *5*, 459–469.
- Pettersen, E.F., Goddard, T.D., Huang, C.C., Couch, G.S., Greenblatt, D.M., Meng, E.C., and Ferrin, T.E. (2004). UCSF Chimera—a visualization system for exploratory research and analysis. *J. Comput. Chem.* *25*, 1605–1612.
- Poirier, M.A., Xiao, W., Macosko, J.C., Chan, C., Shin, Y.K., and Bennett, M.K. (1998). The synaptic SNARE complex is a parallel four-stranded helical bundle. *Nat. Struct. Biol.* *5*, 765–769.
- Rabenstein, M.D., and Shin, Y.K. (1995). Determination of the distance between two spin labels attached to a macromolecule. *Proc. Natl. Acad. Sci. USA* *92*, 8239–8243.
- van Montfort, R.L., Basha, E., Friedrich, K.L., Slingsby, C., and Vierling, E. (2001). Crystal structure and assembly of a eukaryotic small heat shock protein. *Nat. Struct. Biol.* *8*, 1025–1030.
- Yonekura, K., Maki-Yonekura, S., and Namba, K. (2003). Complete atomic model of the bacterial flagellar filament by electron cryomicroscopy. *Nature* *424*, 643–650.